Nonlinear Dynamics (2005) 42: 319–337

Milling Bifurcations from Structural Asymmetry and Nonlinear Regeneration

B. P. MANN[1,3,*], N. K. GARG[1], K. A. YOUNG[2], and A. M. HELVEY[2]

[1]*Nonlinear Dynamics Laboratory, Department of Mechanical and Aerospace Engineering, University of Florida-Gainesville, P.O. Box 116300, FL 32611, U.S.A.;* [2]*Advanced Manufacturing Research and Development, The Boeing Company, St. Louis, MO 63166, U.S.A.;* [3]*Current address: Department of Mechanical & Aerospace Engineering, University of Missouri – Columbia, Engineering Bldg East, Columbia, MO 65203, U.S.A.;* [*]*Author for correspondence (e-mail: bmann@ufl.edu)*

(Received: 14 July 2004; accepted: 8 April 2005)

Abstract. This paper investigates multiple modeling choices for analyzing the rich and complex dynamics of high-speed milling processes. Various models are introduced to capture the effects of asymmetric structural modes and the influence of nonlinear regeneration in a discontinuous cutting force model. Stability is determined from the development of a dynamic map for the resulting variational system. The general case of asymmetric structural elements is investigated with a fixed frame and rotating frame model to show differences in the predicted unstable regions due to parametric excitation. Analytical and numerical investigations are confirmed through a series of experimental cutting tests. The principal results are additional unstable regions, hysteresis in the bifurcation diagrams, and the presence of coexisting periodic and quasiperiodic attractors which is confirmed through experimentation.

Key words: delay differential equations, milling bifurcations, multiple attractors, parametric excitation

1. Introduction

A current trend within major manufacturing industries is the rapid adoption of high-speed milling. For instance, recent improvements by machine tool builders have enabled a paradigm shift within the aerospace community. The new design methodology replaces many labor-intensive sheet metal assemblies with monolithic aluminum components. However, the opportunity to capture substantial cost savings typically requires accurate predictive analysis tools to avoid unstable oscillations, meet dimensional requirements, and to take full advantage of a machining center's capabilities.

A primary limiting factor in material removal applications is the relative oscillations between a cutting tool and workpiece system [1, 2]. More specifically, cutting force models become nonideal energy sources that must capture force modulations created from relative motions between the cutting tool and workpiece system [1, 3]. The most common approach is to prescribe a cutting force model that is a function of the uncut chip area [1, 2, 4]. This type of model connects the relative system oscillations to the cutting forces and chip load variations; these motions can cause dynamic cutting forces and self-excitation of the machine–tool structural modes that lead to instability. Unless avoided, these unstable regions may cause large dynamic loads on the machine spindle and table structure, damage to the cutting tool, and a poor surface finish [1, 2, 5, 6]. Therefore, a key strategy is to apply analytical and numerical methods to predict parameter domains where instabilities exist.

The explanation for machine–tool chatter was first given by Tlusty [7], Tobias [8], and Merritt [9] as "regeneration of waviness." Their research provided the development of stability lobe diagrams that compactly represent the stability information as a function of the control parameters (i.e., spindle speed

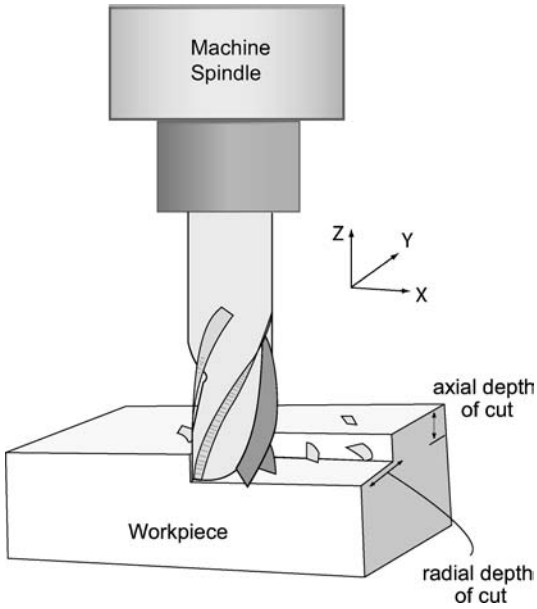

Figure 1. Schematic diagram showing the milling process is an interrupted cutting process.

and depth of cut). An important result from these analyses was the ability to identify stable cutting regions in which larger metal removal rates could be obtained by cutting at higher spindle speeds.

Stability predictions from many early analysis are only approximate for the case of milling, because they rely on the fundamental assumption of continuous cutting. In milling, the cutting forces change direction with tool rotation and cutting is interrupted as each tooth enters and exits the workpiece (see Figure 1). This leads to cutting force coefficients which change from zero (when the tool is free) to large numbers (when the tool is cutting). While numerical simulation can be used to capture the interrupted nature of the milling process [1, 10, 11], the exploration of parameter space by time domain simulation is clearly inefficient.

The focus of many recent investigations has been the occurrence of new bifurcation phenomena in interrupted cutting processes. In addition to Neimark–Sacker or secondary Hopf bifurcations, period-doubling bifurcations have been analytically predicted in references [12–18] and confirmed experimentally in references [5, 12–14, 19–23]. Other investigations have shown additional physical mechanisms which may influence the relative oscillations between the tool and the workpiece [25]. For instance, thermoplastic behavior in chip formation have been reported in reference [26] and frictional effects at the tool–chip interface have been examined in the reference [27].

The original goal of this experimental study was to apply a new analytical approach to a multiple degree-of-freedom system and validate the most common modeling practices. However, initial investigations of the common modeling practices showed strong disagreement with the detailed experimental study. This launched an investigation on the influence of asymmetric structural elements and a further review of the independent cutting tests that were performed to calibrate the unknown parameters of the cutting force model. The outcome of these investigations is much in better agreement, but not perfect agreement, with experiments when certain common modeling practices are not applied. For instance, the presence of asymmetric structural elements and a nonlinear cutting force model show additional unstable parameter domains. A variational equation is formulated to determine the local stability of the nonlinear, nonhomogeneous, delay-differential system from a temporal finite element analysis method.

Experimental and numerical investigations show hysteresis in bifurcation diagrams and the presence of coexisting periodic and quasiperiodic attractors.

2. Model Development

Several alternatives exist for modeling the dynamic behavior of a typical milling process (see Figure 1). For instance, this section develops two different lumped element models: (1) the most common model applied in milling dynamics literature is first described. This model assumes non-rotating restoring and damping forces and a negligible mass imbalance; and (2) the second model applies rotating damping and restoring forces to show structural asymmetry will cause additional parametric excitation terms to appear in the governing equations. In the event that the modal parameters are perfectly symmetric, which is certainly not the case in general practice, the two models will become identical. A schematic of each model considered is shown in Figure 2.

2.1. Fixed Frame Model

The most common approach for investigating the dynamic behavior of the milling process, see references [1, 2, 5, 15, 17, 18, 21, 22, 28], assumes a lumped element model with restoring an damping forces that do not rotate with the cutting tool; this will be called a fixed frame model which typically assumes a negligible mass imbalance. The result of these assumptions can be expressed in the following equation

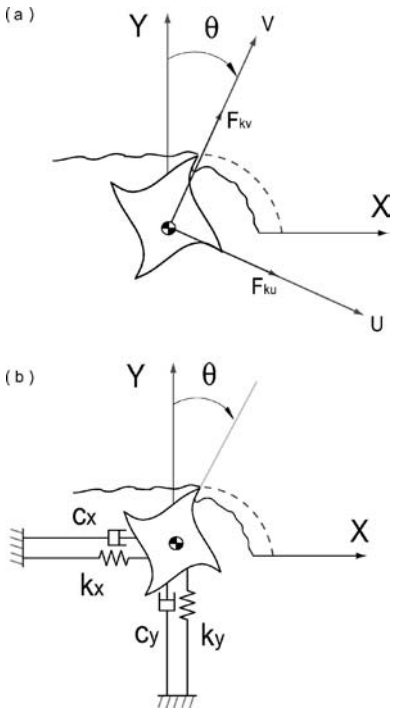

Figure 2. Schematic of two different structural dynamics models: (a) rotating restoring and viscous damping forces; and (b) stationary restoring and damping forces.

form

$$\begin{bmatrix} m & 0 \\ 0 & m \end{bmatrix} \begin{bmatrix} \ddot{x}(t) \\ \ddot{y}(t) \end{bmatrix} + \begin{bmatrix} d_x & 0 \\ 0 & d_y \end{bmatrix} \begin{bmatrix} \dot{x}(t) \\ \dot{y}(t) \end{bmatrix} + \begin{bmatrix} k_x & 0 \\ 0 & k_y \end{bmatrix} \begin{bmatrix} x(t) \\ y(t) \end{bmatrix} = \begin{bmatrix} F_x(x, y, \theta(t), \tau) \\ F_y(x, y, \theta(t), \tau) \end{bmatrix}, \tag{1}$$

where the terms m, $d_{x,y}$, and $k_{x,y}$ are the modal mass, damping, and stiffness in the x- and y-directions of the system. The cutting forces, which are further described in Section 2.3, are written as $F_x(x, y, \theta(t), \tau)$ and $F_y(x, y, \theta(t), \tau)$ to explicitly show their dependence upon the current tool position, the cutter rotation angle, and the tool position in the previous tooth passage (i.e., this necessitates the use of a delayed position variables $x(t-\tau)$ and $y(t-\tau)$, where τ is the time delay between consecutive tooth passages). The generalized lumped element model for this system, which may include the influence of multiple modes along the two orthogonal directions, can be written as

$$\mathbf{M}\ddot{\vec{X}} + \mathbf{D}\dot{\vec{X}} + \mathbf{K}\vec{X} = \vec{F}_c(x, y, \theta(t), \tau)\,, \tag{2}$$

where $\mathbf{M}$, $\mathbf{D}$, and $\mathbf{K}$ are the spatial mass, damping, and stiffness matrices associated with the fixed x- and y-axes and $\vec{F}_c(x, y, \theta(t), \tau)$ is a vector describing the cutting forces.

2.2. Rotating Frame Model

This section derives a governing equation that includes structural asymmetry under the assumption that the damping and restoring force will rotate with the tool; this model is presented to illustrate that additional terms appear in the equation of motion. Since these terms result in a parametrically excited system, which can often alter the stability characteristics of a system, the influence structural asymmetry on stability can be examined. A top view of an end mill whirling at the spindle rotational frequency is shown in Figure 2a. The elastic restoring forces, written as F_{ku} and F_{kv}, are assumed to follow the rotating coordinate frame (u, v). The relationship between the restoring forces in the fixed coordinate frame (F_{kx}, F_{ky}) and the rotating coordinate frame is

$$\begin{bmatrix} F_{ku} \\ F_{kv} \end{bmatrix} = \mathbf{T}(\theta) \begin{bmatrix} F_{kx} \\ F_{ky} \end{bmatrix}. \tag{3}$$

where $\theta(t)$, written as θ, is the cutter rotation angle and $\mathbf{T}(\theta)$ is a rotation matrix defined by

$$\mathbf{T}(\theta) = \begin{bmatrix} \cos\theta(t) & -\sin\theta(t) \\ \sin\theta(t) & \cos\theta(t) \end{bmatrix}. \tag{4}$$

In a similar fashion, the relationship between the displacements in each coordinate system can be written as

$$\begin{bmatrix} u \\ v \end{bmatrix} = \mathbf{T}(\theta) \begin{bmatrix} x \\ y \end{bmatrix}. \tag{5}$$

The influence of rotating asymmetric structural elements is investigated by assuming: (1) the u-direction spring and damping coefficients are $k - \Delta k$ and $d - \Delta d$; and (2) the spring and damping

coefficients in the v-direction are $k + \Delta k$ and $d + \Delta d$. Under the additional assumption of a constant spindle speed, the resulting equation of motion is

$$\begin{bmatrix} m & 0 \\ 0 & m \end{bmatrix} \begin{bmatrix} \ddot{x}(t) \\ \ddot{y}(t) \end{bmatrix} + \begin{bmatrix} d - \Delta d\, \cos 2\theta(t) & \Delta d \sin 2\theta(t) \\ \Delta d \sin 2\theta(t) & d + \Delta d \cos\, 2\theta(t) \end{bmatrix} \begin{bmatrix} \dot{x}(t) \\ \dot{y}(t) \end{bmatrix} + \begin{bmatrix} k - \Delta k\, \cos 2\theta(t) & \Delta k\, \sin 2\theta(t) \\ \Delta k\, \sin 2\theta(t) & k + \Delta k\, \cos 2\theta(t) \end{bmatrix} \begin{bmatrix} x(t) \\ y(t) \end{bmatrix} = \begin{bmatrix} F_x(x, y, \theta(t), \tau) \\ F_y(x, y, \theta(t), \tau) \end{bmatrix}, \tag{6}$$

where m, $d \pm \Delta d$, and $k \pm \Delta k$ are the modal mass, damping, and stiffness terms identified from impact test on a stationary tool. Note that Equation (1) and Equation (6) become identical when the modal parameters are symmetric. A more generalized expression, which may include multiple modes acting along the two orthogonal directions, is given by

$$\mathbf{M}\ddot{\vec{X}} + \mathbf{D}(\theta)\dot{\vec{X}} + \mathbf{K}(\theta)\vec{X} = \vec{F}_c(x, y, \theta(t), \tau). \tag{7}$$

where $\vec{F}_c(x, y, \theta, \tau)$ is the cutting force vector, $\mathbf{M}$, $\mathbf{D}(\theta)$, and $\mathbf{K}(\theta)$ are the spatial mass, damping, and stiffness matrices of the rotating system.

2.3. Cutting Force Model

The cutting forces in a milling operation change direction with tool rotation and cutting is interrupted as each tooth enters and leaves the workpiece (see Figure 1). This leads to cutting force coefficients which change from zero (when the tool is free) to large numbers (when the tool is cutting). The total cutting force in each direction can be written as the summation over the total number of cutting teeth N,

$$\begin{bmatrix} F_x(x, y, \theta(t), \tau) \\ F_y(x, y, \theta(t), \tau) \end{bmatrix} = \sum_{p=1}^{N} g_p(t)\mathbf{T}(\theta)^{-1} \begin{bmatrix} -F_{tp}(x, y, \theta(t), \tau) \\ -F_{rp}(x, y, \theta(t), \tau) \end{bmatrix}. \tag{8}$$

where $g_p(t)$ is a square wave function that provides a discontinuity in the cutting force by assuming a value of one when the p-th tooth is active and zero when this tooth is not cutting. At this point, one could argue that the time intervals for the switching function, $g_p(t)$, could actually depend upon the tool motion. However, it is believed that the application of a constant entry and exit angle does provide a reasonable first approximation that will be further verified with simulation. The tangential and radial cutting force components, $F_{tp}(t)$ and $F_{rp}(t)$ respectively, are considered to be a function of cutting pressures K_t and K_r [1, 2], the axial depth of cut b, and the instantaneous chip thickness $w_p(t)$,

$$F_{tp}(t) = K_t b\, w_p(t)^{\gamma}, \tag{9}$$

$$F_{rp}(t) = K_r b\, w_p(t)^{\gamma}, \tag{10}$$

where $w_p(t)$ depends upon the feed per tooth, h, the cutter rotation angle $\theta_p(t)$, and regeneration in the compliant tool directions. Here, a nonlinear relationship is obtained between the chip thickness and the cutting forces when $\gamma \neq 1$. An approximate expression for the instantaneous chip thickness is

$$w_p(t) \approx h\, \sin\theta_p(t) + [x(t) - x(t - \tau)] \sin\theta_p(t) + [y(t) - y(t - \tau)] \cos\theta_p(t). \tag{11}$$

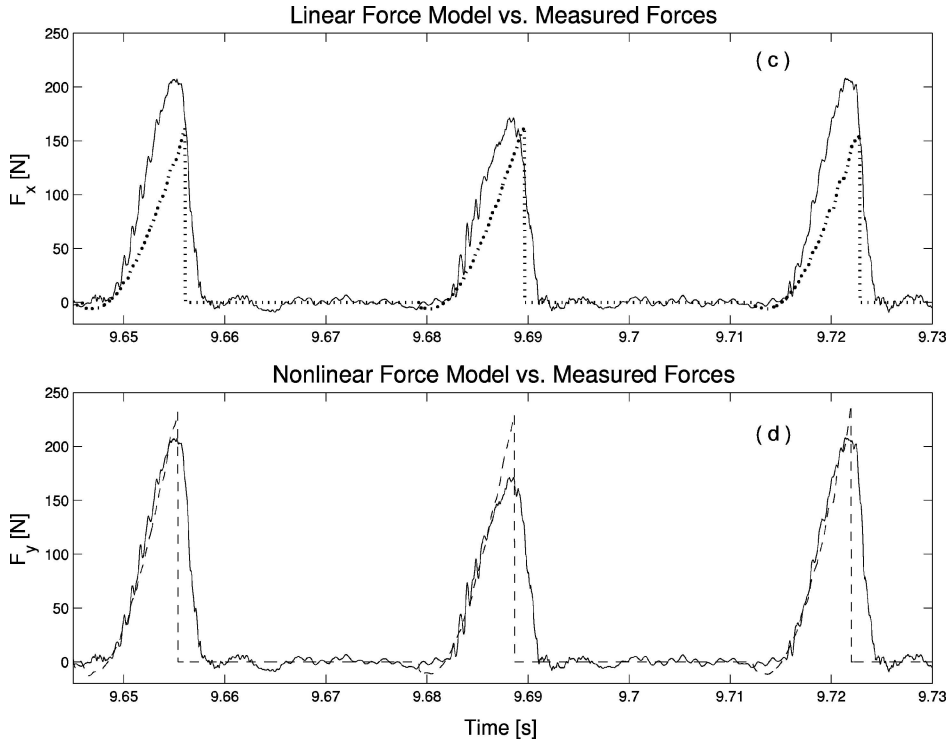

Figure 3. Measured vs. estimated y-direction cutting forces for three consecutive tooth passages made at a depth of cut ($b = 2$ mm) and spindle speed ($\Omega = 900$ rpm) for a two flute 19.05 mm tool. Two comparisons are shown: (c) linear force model (dotted line) vs. measured cutting force data (solid line); and (d) nonlinear force model (dashed line) vs. measured cutting force data (solid line).

where the time delay between consecutive tooth passages is taken to be $\tau = 2\pi/N\Omega$ [s]. Although the relationship shown in Equations (9) and (10) differs from those defined in references [29, 30], similar relationships have been proposed by numerous researchers for turning and drilling studies [1, 31]. Additionally, these expressions provide a particularly convenient connection to the linear model for regeneration – where the linear model, obtained when $\gamma = 1$, can be viewed as a special case of the more general nonlinear relationship.

The proposed nonlinear relationship was investigated after obtaining unsatisfactory results between a linear model and experimental data. For instance, Figure 3 shows a comparison between the proposed force model and the measured cutting forces. Parameter estimates for a linear model only provide a "locally" good fit throughout the cutter rotation (i.e., notice a good fit at cutter entry and a poor fit near cutter exit in Figure 3). If an iterative approach is applied to refine the cutting coefficients, the result is just a shift the location of a good and poor fit. The application the proposed nonlinear relationship, results shown in Figure 3, clearly provides a better correlation to the experimentally observed values. An additional observation that can be made in the graphs is a difference in slope between the analytical cutting forces and the measured cutting forces at tool exit. However, the finite slope shown in the measurement data can actually be attributed to a well-known effect – the discharge time constant of a piezoelectric sensor. These sensors are utilized within the dynamometer to provide measurement capability. Parameters for the nonlinear force model, where both cutting forces and tool displacements were measured for a 19.05-mm diameter tool and aluminum (7050-T7451) workpiece, were estimated

to be $\gamma = 0.94$, $K_{\mathrm{t}} = 7.0 \times 10^8$ [N/m$^{(1+\gamma)}$], $K_{\mathrm{n}} = 2.1 \times 10^8$ [N/m$^{(1+\gamma)}$]. Cutting force measurements were obtained using a Kistler[1] Model 9255B rigid dynamometer and tool displacements were measured with a Lion Precision capacitance probe system.

3. Stability from Solution Perturbation

The models derived in the previous sections illustrate the governing equations for the milling process are discontinuous and contain both periodic coefficients and a time delay. A variational approach is applied here to determine local stability by applying a perturbation, written as $\vec{\xi}(t) = \left[\xi_x(t) \;\; \xi_y(t)\right]^{\mathsf{T}}$, about the desired τ-periodic motion

$$\vec{X}(t) = \vec{X}_p(t) + \vec{\xi}(t) \tag{12}$$

where $\vec{X}_p(t) = \left[x_p(t) \;\; y_p(t)\right]^{\mathsf{T}}$ is the τ-periodic solution. Expanding the nonlinear forces from Equation (8) about the desired periodic motion provides the following after substitution into Equation (5),

$$\mathbf{M}\ddot{\vec{X}}_p + \mathbf{D}(\theta)\dot{\vec{X}}_p + \mathbf{K}(\theta)\vec{X}_p + \mathbf{M}\ddot{\vec{\xi}} + \mathbf{D}(\theta)\dot{\vec{\xi}} + \mathbf{K}(\theta)\vec{\xi} = b\vec{f}_o(\theta) + b\mathbf{K}_c(\theta)[\vec{\xi}(t) - \vec{\xi}(t-\tau)]\,, \tag{13}$$

where $\mathbf{K}_c(\theta)$ and $\vec{f}_o(\theta)$ are compact notation for

$$\mathbf{K}_c(\theta) = \sum_{p=1}^{N} \gamma g_p(t)(h\,\sin\theta_p(t))^{\gamma-1} \begin{bmatrix} -K_t sc - K_r s^2 & -K_t c^2 - K_r sc \\ K_t s^2 - K_r sc & K_t sc - K_r c^2 \end{bmatrix}, \tag{14}$$

$$\vec{f}_o(\theta) = \sum_{p=1}^{N} g_p(t)(h\,\sin\theta_p(t))^{\gamma} \begin{bmatrix} -K_t c - K_r s \\ K_t s - K_r c \end{bmatrix}, \tag{15}$$

with $s = \sin\theta_p(t)$ and $c = \cos\theta_p(t)$.

While perturbation growth will result in an unstable solution, perturbation decay (i.e., $\vec{\xi}(t) = 0$) will yield a stable periodic solution to the following equation

$$\mathbf{M}\ddot{\vec{X}}_p + \mathbf{D}(\theta)\dot{\vec{X}}_p + \mathbf{K}(\theta)\vec{X}_p = b\vec{f}_o(\theta). \tag{16}$$

Equation (16) describes a linear system with a τ-periodic excitation term and a τ-periodic solution. Subtracting Equation (16) from Equation (13) results in an equation for the perturbed motion

$$\mathbf{M}\ddot{\vec{\xi}}(t) + \mathbf{D}(\theta)\dot{\vec{\xi}}(t) + \mathbf{K}(\theta)\vec{\xi}(t) = b\mathbf{K}_c(\theta)[\vec{\xi}(t) - \vec{\xi}(t-\tau)]. \tag{17}$$

3.1. Discrete Map Development

This section describes the development of a discrete map for the resulting variational system given by Equation (17). The most general case of a low radial immersion process, where the radial immersion

[1] Commercial equipment is identified for completeness and does not imply endorsement by the authors.

is defined as the radial engagement divided by the tool diameter, is handled by a temporal finite element approach to match solutions between cutting and non-cutting regimes. The previous work for applications to fixed-frame systems with linear force models is described in references [5, 18, 23, 24].

When the tool is out of contact with the workpiece, the system is governed by the equation for free vibration

$$\mathbf{M}\ddot{\vec{\xi}}(t) + \mathbf{D}(\theta)\dot{\vec{\xi}}(t) + \mathbf{K}(\theta)\vec{\xi}(t) = 0. \tag{18}$$

This equation can be rearranged into state-space form

$$\begin{bmatrix} \dot{\vec{\xi}}(t_{\mathrm{f}}) \\ \ddot{\vec{\xi}}(t_{\mathrm{f}}) \end{bmatrix} = \Phi(t_{\mathrm{f}}, 0) \begin{bmatrix} \vec{\xi}(0) \\ \dot{\vec{\xi}}(0) \end{bmatrix}, \tag{19}$$

where t_{f} is the duration for free vibration and $\mathbf{\Phi}(t_f, 0)$ is a state transition matrix that relates the states of the perturbation at the beginning of free vibration to the perturbed states at the end of free vibration.

During the cutting process, there is no exact solution for the perturbed motion. However, we can divide the cutting time into elements and approximate the perturbation as a linear combination of polynomials

$$\vec{\xi}(t) = \sum_{i=1}^{4} \vec{a}_{ji}^{\,n} \phi_i(\sigma_j(t)) \tag{20}$$

Here $\sigma_j(t) = t - n\tau - \sum_{k=1}^{j-1} t_k$ is the "local" time within the j-th element of the n-th period, the time span for the k-th element is t_k and the trial functions or polynomial are written as $\phi_i(\sigma_j(t))$.

Substitution of the assumed solution (Equation (20)) into the variational equation leads to a non-zero error. The error from the assumed solution is "weighted" by multiplying by a set of test functions and setting the integral of the weighted error to zero to obtain two equations per element [32, 33],

$$\begin{aligned} \int_0^{t_j} \Bigg[& \mathbf{M}\left(\sum_{i=1}^{4} a_{ji}^{n} \ddot{\phi}_i(\sigma_j)\psi_r(\sigma_j) \right) + \mathbf{D}(\sigma_j)\left(\sum_{i=1}^{4} a_{ji}^{n} \dot{\phi}_i(\sigma_j)\psi_r(\sigma_j) \right) \\ & + (\mathbf{K}(\sigma_j) - b\mathbf{K}_c(\sigma_j))\left(\sum_{i=1}^{4} a_{ji}^{n} \phi_i(\sigma_j)\psi_r(\sigma_j) \right) \\ & + b\mathbf{K}_c(\sigma_j)\left(\sum_{i=1}^{4} a_{ji}^{n-1} \phi_i(\sigma_j)\psi_r(\sigma_j) \right) \Bigg] d\sigma_j \; = 0, \quad r = 1, 2, \end{aligned} \tag{21}$$

The test functions are chosen to be: $\psi_1(\sigma_j) = 1$ (constant) and $\psi_2(\sigma_j) = \sigma_j/t_j - 1/2$ (linear). The integrals, shown in Equation (21), are taken over the time for each element, $t_j = t_{\mathrm{c}}/E$, thereby dividing the time in the cut t_c into E elements. The terms $\mathbf{D}(\sigma_j)$, $\mathbf{K}(\sigma_j)$, and $\mathbf{K}_c(\sigma_j)$ have been used in place of the previously defined $\mathbf{D}(\theta)$, $\mathbf{K}(\theta)$, and $\mathbf{K}_c(\theta)$ to explicitly show their dependence on the local time within each element. The state transition matrix and the equations for each element, Equation (21), can be arranged into a global matrix relating the coefficients of the states in the current period to the

coefficients of the states in previous period. The following expression is for the case when the number of elements is three

$$\begin{bmatrix} \mathbf{I} & \mathbf{0} & \mathbf{0} & \mathbf{0} \\ \mathbf{N}_1^1 & \mathbf{N}_2^1 & \mathbf{0} & \mathbf{0} \\ \mathbf{0} & \mathbf{N}_1^2 & \mathbf{N}_2^2 & \mathbf{0} \\ \mathbf{0} & \mathbf{0} & \mathbf{N}_1^3 & \mathbf{N}_2^3 \end{bmatrix} \begin{bmatrix} \vec{a}_{11} \\ \vec{a}_{12} \\ \vec{a}_{21} \\ \vec{a}_{22} \\ \vec{a}_{31} \\ \vec{a}_{32} \\ \vec{a}_{33} \\ \vec{a}_{34} \end{bmatrix}^n = \begin{bmatrix} \mathbf{0} & \mathbf{0} & \mathbf{0} & \mathbf{\Phi} \\ \mathbf{P}_1^1 & \mathbf{P}_2^1 & \mathbf{0} & \mathbf{0} \\ \mathbf{0} & \mathbf{P}_1^2 & \mathbf{P}_2^2 & \mathbf{0} \\ \mathbf{0} & \mathbf{0} & \mathbf{P}_1^3 & \mathbf{P}_2^3 \end{bmatrix} \begin{bmatrix} \vec{a}_{11} \\ \vec{a}_{12} \\ \vec{a}_{21} \\ \vec{a}_{22} \\ \vec{a}_{31} \\ \vec{a}_{32} \\ \vec{a}_{33} \\ \vec{a}_{34} \end{bmatrix}^{n-1}, \tag{22}$$

where the sub-matrices and elements of the sub-matrices for the j-th element are

$$\mathbf{N}_1^j = \begin{bmatrix} \mathbf{N}_{11}^j & \mathbf{N}_{12}^j \\ \mathbf{N}_{21}^j & \mathbf{N}_{22}^j \end{bmatrix}, \quad \mathbf{N}_2^j = \begin{bmatrix} \mathbf{N}_{13}^j & \mathbf{N}_{14}^j \\ \mathbf{N}_{23}^j & \mathbf{N}_{24}^j \end{bmatrix}, \tag{23}$$

$$\mathbf{P}_1^j = \begin{bmatrix} \mathbf{P}_{11}^j & \mathbf{P}_{12}^j \\ \mathbf{P}_{21}^j & \mathbf{P}_{22}^j \end{bmatrix}, \quad \mathbf{P}_2^j = \begin{bmatrix} \mathbf{P}_{13}^j & \mathbf{P}_{14}^j \\ \mathbf{P}_{23}^j & \mathbf{P}_{24}^j \end{bmatrix}, \tag{24}$$

$$N_{ri}^j = \int_0^{t_j} \left[\mathbf{M}\ddot{\phi}_i(\sigma_j) + \mathbf{D}(\sigma_j)\dot{\phi}_i(\sigma_j) + (\mathbf{K}(\sigma_j) - b\mathbf{K}_c(\sigma_j))\phi_i(\sigma_j)\right]\psi_r(\sigma_j)\, d\sigma_j, \tag{25}$$

$$P_{ri}^j = \int_0^{t_j} -b\mathbf{K}_c(\sigma_j)\phi_i(\sigma_j)\psi_r(\sigma_j)\, d\sigma_j. \tag{26}$$

Equation (22) describes a discrete dynamical system, or map, that can be written as

$$\mathbf{A}\vec{a}_n = \mathbf{B}\vec{a}_{n-1}, \quad \text{or} \quad \vec{a}_n = \mathbf{Q}\vec{a}_{n-1}. \tag{27}$$

where the transition matrix is given by $\mathbf{Q} = \mathbf{A}^{-1}\mathbf{B}$. Since this result depends upon the inversion of $\mathbf{A}$, we have performed numerical investigations that show this matrix is invertible unless very large values of b are examined – such as 1 (m). However, it would be physically impossible to cut at such depths with present day machines and cutting tool materials.

3.2. Stability Prediction

The eigenvalues of the transition matrix, $\mathbf{Q}$, are the dynamic map characteristic multipliers (CMs) that contain local stability information [34]. The condition for stability requires the CM magnitudes to be in a modulus of less than one for a given spindle speed (Ω) and depth of cut (b) for an asymptotically stable milling process. Figure 4 shows the boundaries between stable and unstable cutting as a function of spindle speed and depth of cut.

Two distinct types of instabilities are illustrated by CM trajectories in the complex plane: (1) a flip bifurcation or period doubling phenomena occurs when a negative real CM passes through the unit circle; and (2) a Neimark–Sacker or secondary Hopf bifurcation occurs when a complex CM obtains a magnitude greater than one. These routes to instability are illustrated in the bottom graphs of Figure 4 with the corresponding speed and depth of cut points shown in the top stability chart. One particularly interesting result from this diagram is an abrupt jump in the largest eigenvalue just

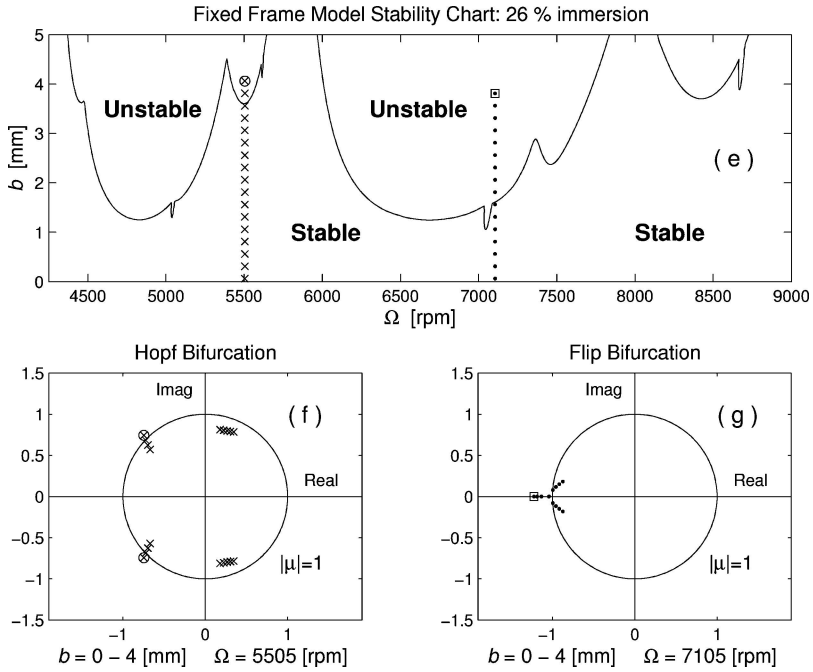

Figure 4. Stability is predicted from characteristic multiplier magnitudes. Unstable parameter combinations penetrate the unit circle in the complex plane: (e) down-milling stability predictions; and (f) characteristic multiplier trajectories for a discontinuous Hopf bifurcation ($\Omega = 5505$ rpm, $b = 0$–4 mm); and (g) characteristic multiplier trajectories for a flip bifurcation ($\Omega = 7105$ rpm, $b = 0$–4 mm). Modal parameters for this system are listed in Table 1.

prior to the occurrence of a secondary Hopf bifurcation. This type of eigenvalue discontinuity is often problematic when attempting to optimize parameter selection and can be attributed to the fact that $\mathbf{Q}$ is asymmetric [36]. The first two modes of vibration in the x- and y-direction of Figure 1, identified from impact test on a cutting tool, were used to construct this stability chart. The modal parameters, listed in Table 1, were assumed identical (symmetric) in each direction of the tool for the presented results; this corresponds to the fixed frame model, given by Equation (7), with four degrees of freedom.

As a second example, the model presented in Equation (6) is used to study the role of structural asymmetry; these results are shown in Figure 5. To create the stability lobes shown in this graph, the modal parameters listed in Table 2 were utilized and the value of stiffness asymmetry, given by Δk, was

Table 1. Single direction structural modes.

Diameter (mm)	M (kg)		D (Ns/m)		K (N/m)$\times 10^6$	
19.05	0.6519	0.000	36.87	0.000	0. 8783	0.000
	0.000	0.2242	0.000	43.67	0.0000	2.1987

Table 2. Modal parameters for asymmetry study.

Diameter (mm)	m (kg)	d (Ns/m)	k (N/m)
19.05	0.061	4.092	1.668×10^6

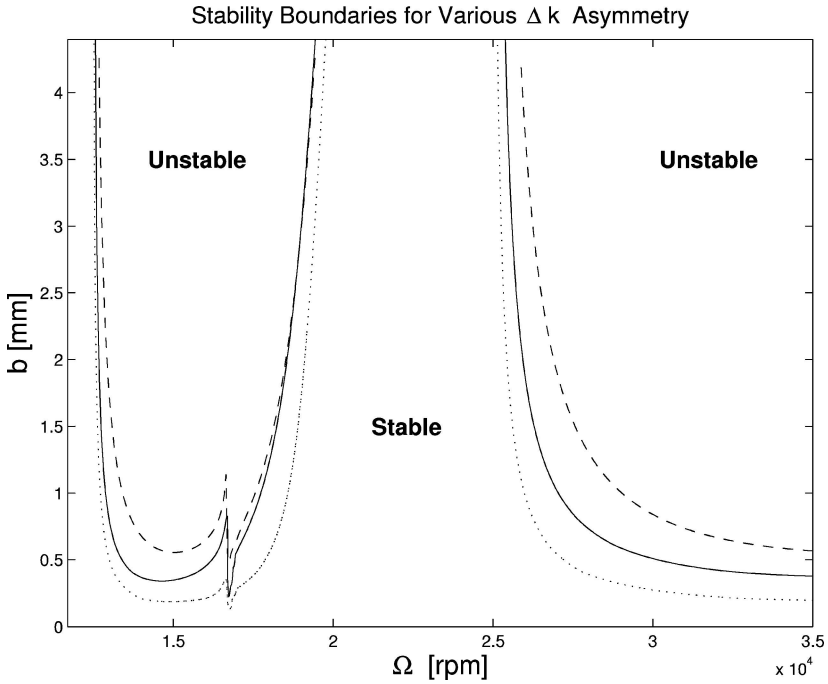

Figure 5. Nonlinear regeneration model stability boundaries for three different magnitudes of asymmetry in the modal stiffness (Δk). The various levels of asymmetry are denoted by: (1) dashed line is $\Delta k = 0$; (2) solid line is $\Delta k = 0.05k$; and (3) dotted line is $\Delta k = 0.10k$. The radial immersion was set to 5% and modal parameters for this system are listed in Table 2.

varied while taking the value of Δd to be zero. An important observation from this graph is the additional unstable regions that occur due with an increase in the cutting tool asymmetry. The explanation for the added unstable regions lies in the introduction of the asymmetric modal parameters, captured by Δk in Equation (6), which provide a parametric excitation to couple the motions in the x- and y-directions of the system [35].

Since the results presented within this section do not account for a loss of contact between the cutting tool and workpiece, it is relevant to examine the behavior of the milling process through simulation. The next section provides a discussion of loss of contact and describes how the resulting behavior is investigated.

3.3. Bifurcation and Hysteresis

Relative oscillations between the cutting tool and workpiece system will initially grow in an unstable cutting process. As the relative oscillations build, cutting forces will also grow until the tool jumps out of the cut. As the tool jumps out of the cut, the cutting forces become zero and free vibrations occur until the tool re-enters the cut. The result of this nonlinearity is bounded post-bifurcation behavior that occurs as the tool continues to reenter and jump out of the cut [5]. This basic nonlinearity, associated with the tool jumping out of the cut, is not captured by the equations defined earlier. However, this post-bifurcation behavior can be captured in numerical integration by: (1) setting the cutting forces to zero when negative values of the radial chip thickness $w_p(t)$ arise; and (2) updating the delayed position of the tool, defined earlier as the displacement of the tool from the previous tooth passage, to be a value

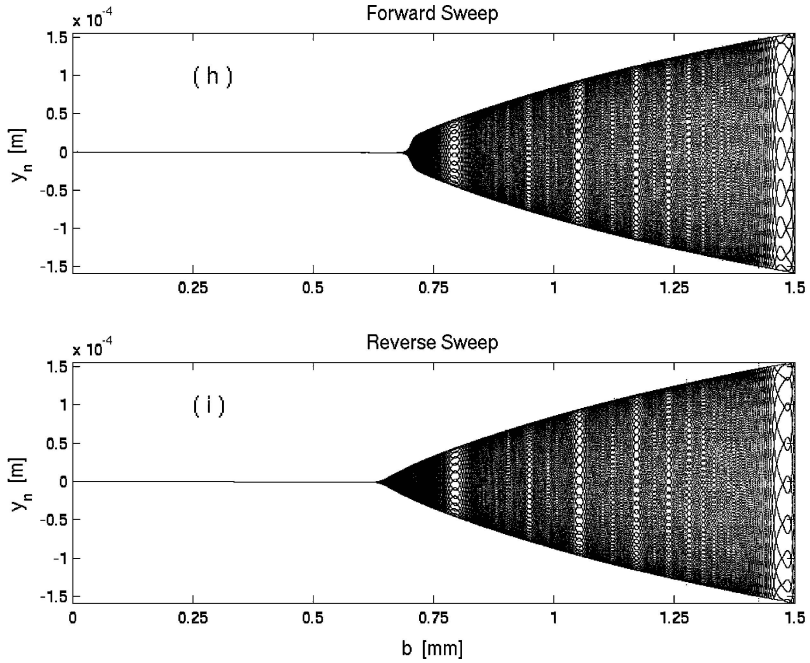

Figure 6. Numerical integration bifurcation diagrams for the experimental system described in Table 3. Results show τ-periodic samples of y-direction displacements, labeled as y_n, for a cutting speed of $\Omega = 35,000$ rpm. The nonlinear force model shows hysteresis in the bifurcation diagrams when comparing the: (h) forward sweep; and (i) reverse sweep cases.

from the last revolution where cutting occurred at the specific angular position of interest. Another alternative for capturing the post-bifurcation behavior is to re-mesh the time domain (i.e., truncate the temporal elements with discontinuities) while using the same criteria for negative $w_p(t)$ values and the values of the previously machined surface [5].

Figure 6 shows a forward and reverse sweep bifurcation diagram for the experimental system studied in Section 5. This graph was created by varying a control parameter, the depth of cut b, during numerical integration of Equation (4) while capturing τ-periodic samples of the y-direction displacements. An interesting result from the nonlinear force model is the presence of hysteresis in these graphs; this gives a clear indication that multiple attractors can coexist for certain parameter combinations. The numerical settings used for the simulation were 1000 time steps per revolution, 100,000 cutter revolutions, and the depth of cut was varied linearly.

4. Equilibria Solutions

Parameter selection based entirely upon stability considerations is often inadequate for the production of precision components. Specifically, certain stable parameter combinations can still result in an inaccurately machined surface. This can occur because the amplitude and phasing of cutter oscillations is dependent upon the cutting process parameters (i.e., spindle speed (Ω), axial depth of cut (b), and tool feed (h)). Another possible reason to further study the predicted stable solutions, which is not further explored here, is the presence of a small-amplitude repelling limit cycle around the stable cutting solutions. The intent of this section is to describe an approach for equilibria solution prediction from

the formulation of a dynamic map – the additional decision making information necessary for *a priori* parameter selection.

An asymptotically stable cutting process results from perturbation decay. The remaining dynamical system, described by Equation (16), now contains an ideal energy source. Discretizing this equation, by following the approach outlined in Section 3, results in

$$\begin{bmatrix} \mathbf{I} & \mathbf{0} & \mathbf{0} & \mathbf{0} \\ \mathbf{N}_1^1 & \mathbf{N}_2^1 & \mathbf{0} & \mathbf{0} \\ \mathbf{0} & \mathbf{N}_1^2 & \mathbf{N}_2^2 & \mathbf{0} \\ \mathbf{0} & \mathbf{0} & \mathbf{N}_1^3 & \mathbf{N}_2^3 \end{bmatrix} \begin{bmatrix} \vec{a}_{11} \\ \vec{a}_{12} \\ \vec{a}_{21} \\ \vec{a}_{22} \\ \vec{a}_{31} \\ \vec{a}_{32} \\ \vec{a}_{33} \\ \vec{a}_{34} \end{bmatrix}^n = \begin{bmatrix} \mathbf{0} & \mathbf{0} & \mathbf{0} & \mathbf{\Phi} \\ \mathbf{0} & \mathbf{0} & \mathbf{0} & \mathbf{0} \\ \mathbf{0} & \mathbf{0} & \mathbf{0} & \mathbf{0} \\ \mathbf{0} & \mathbf{0} & \mathbf{0} & \mathbf{0} \end{bmatrix} \begin{bmatrix} \vec{a}_{11} \\ \vec{a}_{12} \\ \vec{a}_{21} \\ \vec{a}_{22} \\ \vec{a}_{31} \\ \vec{a}_{32} \\ \vec{a}_{33} \\ \vec{a}_{34} \end{bmatrix}^{n-1} + \begin{bmatrix} \vec{0} \\ \vec{0} \\ \vec{C}_1^1 \\ \vec{C}_2^1 \\ \vec{C}_1^2 \\ \vec{C}_2^2 \\ \vec{C}_1^3 \\ \vec{C}_2^3 \end{bmatrix}, \tag{28}$$

where the sub-matrices and elements of the sub-matrices are given in Equations (23) and (25). The remaining term required for equilibria solution prediction is

$$C_p^j = \int_0^{t_j} b \vec{f}_o(\sigma_j) \psi_p(\sigma_j) \, d\sigma_j. \tag{29}$$

Equation (28) can be written as

$$\vec{a}_n = \mathbf{Q} \vec{a}_{n-1} + \vec{D}, \tag{30}$$

after multiplying by the inverse of the matrix on the left hand side. The coefficient vector $\vec{a}_n$ identifies the velocity and displacement at the beginning and end of each element. Surface location error is given by the displacement coefficient value when the cutting tooth is normal to the surface. With the assumption of no tool helix angle, this occurs at cutter entry into the cut for up-milling and cutter exit for down-milling.

Stable milling processes have τ-periodic cutting forces and τ-periodic solutions. The steady state coefficients are found from the fixed points ($\vec{a}_n^*$) of the dynamic map

$$\vec{a}_n = \vec{a}_{n-1} = \vec{a}_n^*. \tag{31}$$

Substitution of Equation (31) into Equation (30) gives the fixed point map solution or steady-state coefficient vector

$$\vec{a}_n^* = (\mathbf{I} - \mathbf{Q})^{-1} \vec{D}. \tag{32}$$

Since $\mathbf{Q}$ and $\vec{D}$ can be computed exactly for each spindle speed and depth of cut, the fixed point displacement solution can be found and used to specify surface location error as a function of machining process parameters.

5. Experimental Stability Test

A five-axis linear motor Ingersol machining center with a Fischer, 40,000 rpm and 40-kW spindle was used to perform stability cutting tests with the two-flute, 19.05 mm diameter, 106 mm overhang, end mill. Modal parameters for the experimental system were obtained from impact tests at the cutter tip (see Table 3). An aluminum (7050-T7451) workpiece was down-milled at a 5% radial immersion and a feedrate of $h = 0.178$ (mm/tooth); the spindle speed (Ω) and depth of cut (b) were changed for each cutting test to determine the onset of unstable vibrations. Since multiple cuts were performed on the same workpiece, a clean-up pass was performed prior to every recorded cut to create a reliable reference surface.

Tool displacements, measured approximately 22 mm from the tool tip, were recorded at a rate of 25 KHz per channel using a laptop data acquisition system and Lion Precision capacitance probes (see Figure 7). A once per revolution timing signal was measured, using a laser tachometer, to read a barcode that was painted onto the non-fluted segment of the tool. Experimental stability results have been superimposed onto the stability predictions for the fixed-axis model in Figure 8 and the rotational dynamics model in Figure 9. Stability test, labeled as cases A–G, are further examined in Figures 10 and 11. However, before diverting the attention away from Figures 8 and 9, it is worthy to note that there are several regions where the nonlinear model for regeneration provides a much better match with experiment and the differences between fixed frame and rotating frame stability predictions are nearly insignificant.

Raw displacement measurements were periodically sampled at the tooth passage frequency to create 1/tooth passage displacement samples and Poincaré sections shown in displacement versus delayed displacement coordinates; these plots are also shown with the power spectral density (PSD) of the continuously sampled displacement in Figure 10. Tests were declared stable if the 1/tooth passage sampled displacement, or τ-periodic samples, approached a fixed point value (see Figure 10, case A).

Unstable behavior predicted by complex characteristic multipliers with a magnitude greater than one, shown by case B, corresponds to Neimark–Sacker or secondary Hopf bifurcation. This post-bifurcation

Table 3. Modal parameters for experimental system.

Diameter (mm)	m (Kg)	d (Ns/m)	Δd (Ns/m)	k (N/m)	Δk (N/m)
19.05	0.061	4.092	0.234	1.668×10^6	-1.223×10^3

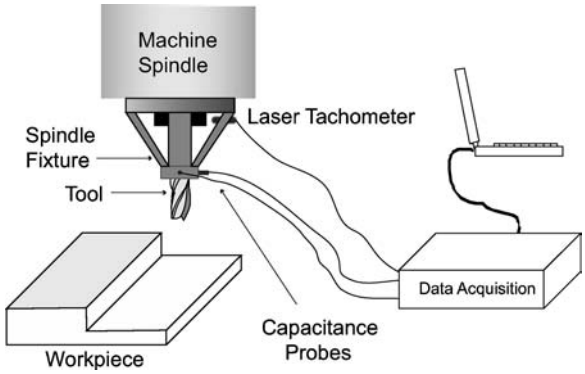

Figure 7. Schematic diagram of test and measurement system used for milling experiments.

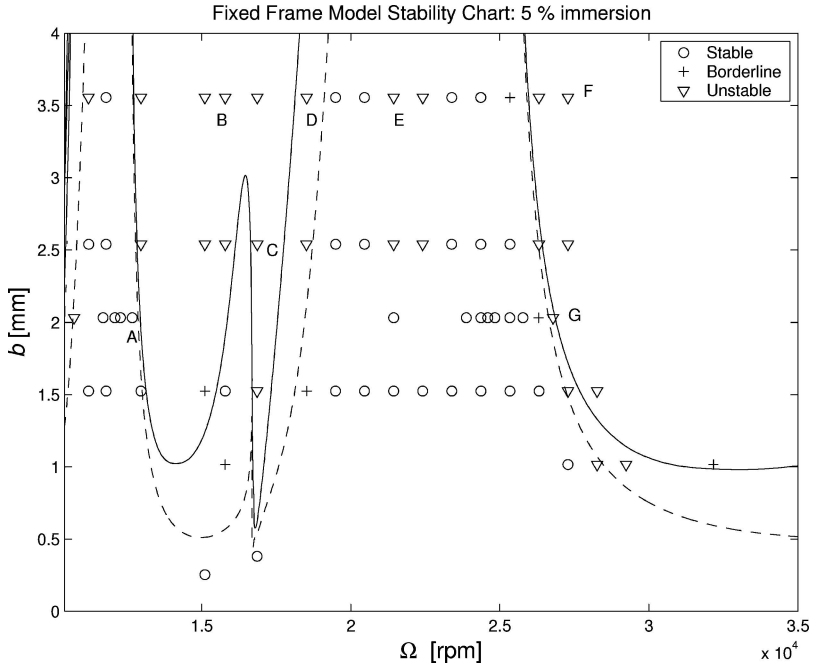

Figure 8. Down-milling experimental results vs. fixed frame model stability predictions for the 19.05 mm tool described in Table 3. Linear regeneration model stability boundaries are shown by a solid line and nonlinear regeneration model stability boundaries are shown by a dotted line. Symbols in the above diagram are as follows: (1) ($\circ$) is a clearly stable case; (2) ($\triangledown$) is an unstable cutting test; and 3) $+$ is a borderline unstable case (i.e., not clearly stable or unstable).

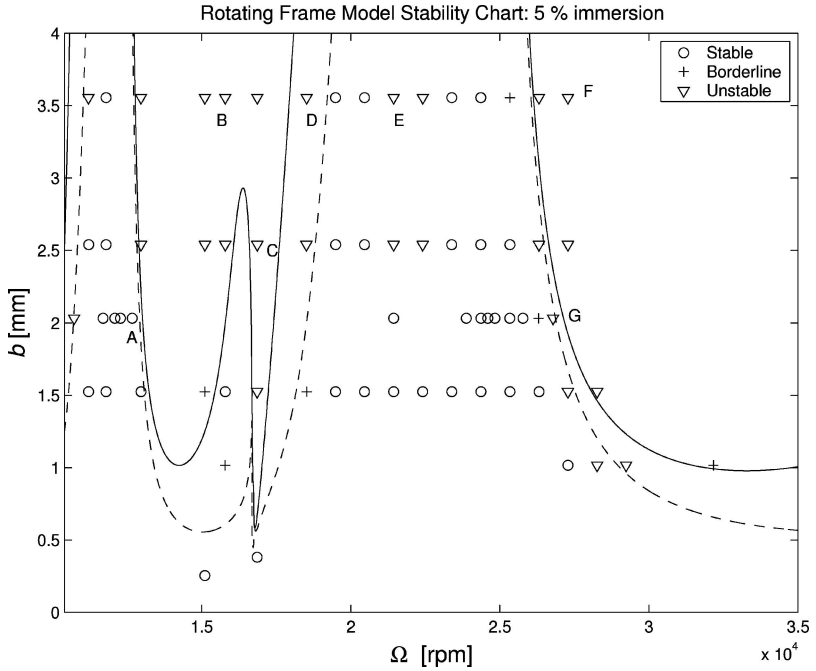

Figure 9. Down-milling experimental results vs. rotating frame model stability predictions for the 19.05 mm tool described in Table 3. Linear regeneration model stability boundaries are shown by a solid line and nonlinear regeneration model stability boundaries are shown by a dotted line. Symbols in the above diagram are as follows: (1) ($\circ$) is a clearly stable case; (2) ($\triangledown$) is an unstable cutting test; and 3) $+$ is a borderline unstable case (i.e., not clearly stable or unstable).

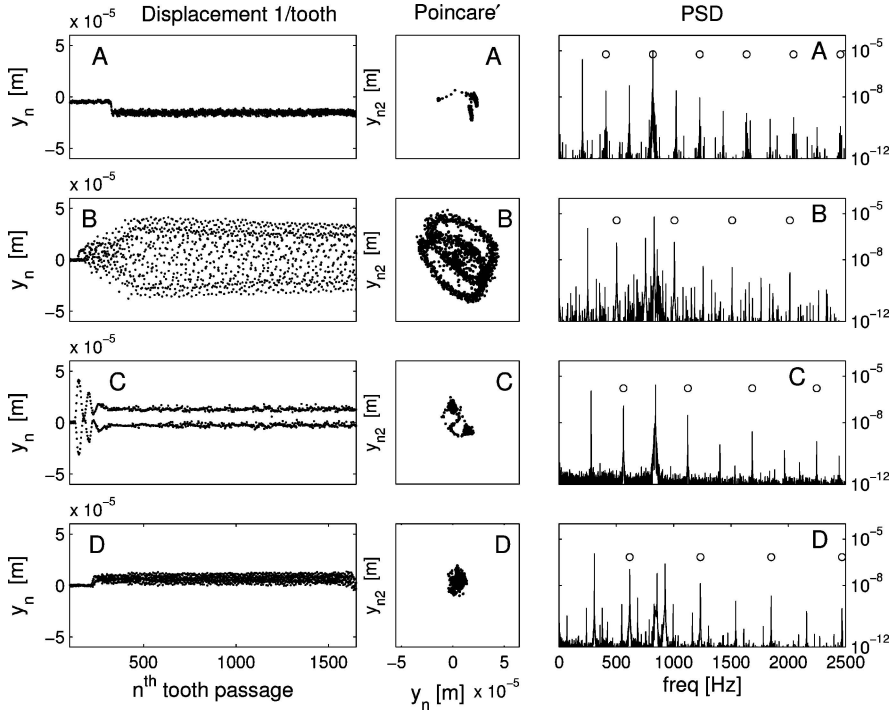

Figure 10. Experimental down-milling measurement data for cases (A, B, C, and D) shown in Figures 8 and 9. Each row contains a y-axis 1/tooth displacement plot, a Poincaré section shown in displacement (y_n) vs. delayed displacement (y_{n2}) coordinates, and the tooth passing frequency is marked by ($\circ$) on the power spectrum (PSD). A stable process is shown for Case A ($\Omega = 12285$ rpm, $b = 2.0$ mm). Unstable cutting processes are shown in Cases B ($\Omega = 15112$ rpm, $b = 3.6$ mm), C ($\Omega = 16868$ rpm, $b = 2.5$ mm), and D ($\Omega = 18516$ rpm, $b = 3.6$ mm). Cases B and D result from unstable Neimark–Sacker or secondary Hopf bifurcations and Case D shows a flip bifurcation.

test result shows the 1/tooth-passage displacement samples are incommensurate with the tooth passage frequency and quasiperiodic motions can be observed in the Poincaré sections. Due to static and dynamic runout in the cutter teeth, multiple circular rings appear in the Poincaré sections – a separate circle for each cutting tooth. Since the resulting sequential mapping from one cutting tooth to the next is predicted to be uniform in the absence of cutter runout, these tests provide further insight about the role of runout in the dynamic tool motions. Case D is particularly interesting since unstable behavior is only predicted by the nonlinear regeneration model ($\gamma \neq 1$). Additionally, the PSD frequency content shows transitional behavior between the predicted Neimark–Sacker and period doubling bifurcation regions (i.e., spectra peaks appear at both half intervals of the tooth passage frequency and at other incommeasurate frequencies).

Unstable period-doubling behavior, commonly referred to as a flip bifurcation [5, 12, 19, 20, 22, 23], is predicted when the dominant characteristic multiplier of the discrete map model is negative and real with a magnitude greater than one. Experimental evidence of this type of post-bifurcation behavior is shown by case C of Figure 10.

An example cutting test that does not agree with either model is shown by case E of Figure 11. The experimental 1/tooth-passage displacement samples, Poincaré section, and PSD graph clearly indicates post-bifurcation behavior – where both the linear and nonlinear models predict stable machining. Case F confirms the predicted unstable region at the higher spindle range for both structural models. The cutting

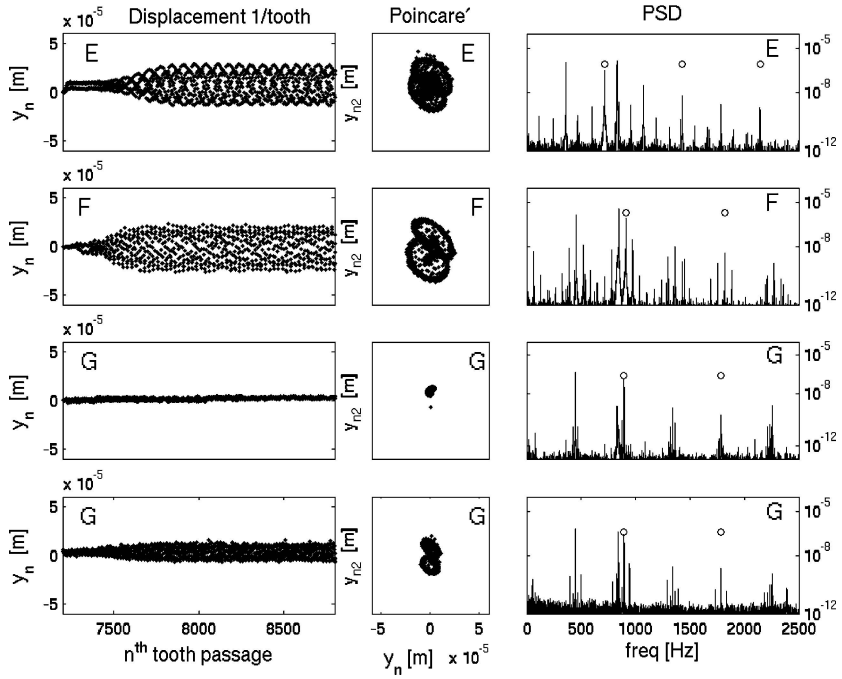

Figure 11. Experimental down-milling measurement data for cases (E, F, and G) shown in Figures 8 and 9. Each row contains a y-axis 1/tooth displacement plot, a Poincaré section shown in displacement (y_n) vs. delayed displacement (y_{n2}) coordinates, and the tooth passing frequency is marked by ○ on the power spectrum (PSD). Quasiperiodic motions arise in the post-bifurcation behavior of Cases E ($\Omega = 21439$ rpm, $b = 3.6$ mm) and F ($\Omega = 27285$ rpm, $b = 3.6$ mm). Repeated test for Case G ($\Omega = 26796$ rpm, $b = 2.0$ mm) provides experimental evidence of multiple attractors and a sensitivity to initial conditions.

test for the final example, represented by case G, were repeated four times with two stable and two unstable outcomes (see examples in the bottom two graphs of Figure 11). These results provide experimental evidence of a sensitivity to initial conditions and the coexistence of a periodic and quasiperiodic attractor.

6. Conclusions

Several alternatives exist to model the complex dynamical behavior of a high-speed milling processes. This paper investigates the choice between a typical fixed-axis model and a model for rotating structural elements. A variational system is formulated from a nonlinear relationship observed during experimental test that provides a general relationship between the tool feed rate and cutting forces. Stability is determined for the time-varying system by expanding the perturbed periodic solution about the stable periodic motion. This provides a suitable delay-differential equation for temporal finite element analysis. The temporal finite element method forms an approximate solution by dividing the time in the cut into a finite number of elements. The approximate solution is then matched with the exact solution for free oscillations to obtain a discrete map. Stability is determined directly from the eigenvalues of map characteristic multipliers. Since parameter selection based entirely upon stability considerations is often inadequate in the production of precision components, an approach to determine equilibria solutions is described.

Initial investigations of the common modeling practices showed strong disagreement with the detailed experimental study. This served as the motivation for the current study, the inclusion of a nonlinear force model, which has provided much better agreement between experimentally observed behavior and analytical predictions. It is additionally shown that asymmetric structural elements can cause added unstable regions due to the coupling of parametric excitation terms in the rotating system, but only small asymmetries are observed in the particular experimental system examined. Also, despite the many cases that appear to be in direct agreement with predictions, some differences were still observed between analysis and experiment. Additional steps were taken to investigate these differences by relaxing the assumption for the switching function, $g_p(t)$, through numerical simulation. However, this did not change the outcome of the predictions and it is believed the primary differences between experiment and analysis are related to: (1) relative motions from frictional and/or thermoplastic effects; (2) the assumption that measured cutting coefficients are unaffected by changes in spindle speed; or (3) neglecting the helix angle of the cutting tool.

Acknowledgements

Support from U.S. National Science Foundation CAREER Award (CMS-0348288) and The Boeing Company is gratefully acknowledged. Additionally, the authors would like to thank both Gábor Stépán and Tamás Insperger, from the Budapest University of Technology and Economics, for their commentary on the presented work.

References

1. Tlusty, J., *Manufacturing Processes and Equipment*, 1st edn., Prentice Hall, Upper Saddle River, NJ, 2000.
2. Altintas, Y., *Manufacturing Automation*, 1st edn., Cambridge University Press, New York, 2000.
3. Nayfeh, A. H. and Mook, D. T., *Nonlinear Oscillations*, Wiley, New York, 1979.
4. Davies, M. and Balachandran, B. 'Impact dynamics in milling of thin-walled structures', *Nonlinear Dynamics* **22**, 2001, 375–392.
5. Mann, B. P., Bayly, P. V., Davies, M. A., and Halley, J. E., 'Limit cycles, bifurcations, and accuracy of the milling process', *Journal of Sound and Vibration* **277**, 2004, 31–48.
6. Doi, S. and Kato, S. 'Chatter vibration of lathe tools', *Transactions of the ASME* **78**, 1956, 1127–1134.
7. Tlusty, J., Polacek, A., Danek, C., and Spacek, J., *Selbsterregte Schwingungen an Werkzeugmaschinen*, VEB Verlag Technik, Berlin, 1962.
8. Tobias, S. A., *Machine Tool Vibration*, Blackie, London, 1965.
9. Merritt, H., 'Theory of self-excited machine tool chatter', *Journal of Engineering for Industry* **87**(4), 1965, 447–454.
10. Smith, S. and Tlusty, J., 'An overview of the modeling and simulation of the milling process', *Journal of Engineering for Industry* **113**, 1991, 169–175.
11. Montgomery, D. and Altintas, Y., 'Mechanism of cutting force and surface generation in dynamic milling', *Journal of Engineering for Industry* **113**, 1991, 160–168.
12. Davies, M. A., Pratt, J. R., Dutterer, B., and Burns, T. J., 'Stability prediction for low radial immersion milling', *Journal of Manufacturing Science and Engineering* **124**(2), 2002, 217–225.
13. Davies, M. A., Pratt, J. R., Dutterer, B., and Burns, T. J., 'The stability of low immersion milling', *Annals of the CIRP* **49**, 2000, 37–40.
14. Bayly, P. V., Halley, J. E., Mann, B. P., and Davies, M. A., 'Stability of interrupted cutting by temporal finite element analysis', in *Proceedings of the 18th Biennial Conference on Mechanical Vibration and Noise,* Pittsburg, PA, 2001.
15. Insperger, T. and Stépán, G., 'Stability of high-speed milling', in *Proceedings of Symposium on Nonlinear Dynamics and Stochastic Mechanics*, Orlando, FL, AMD-241, 2000, pp. 119–123.
16. Corpus, W. T. and Endres, W. J., 'A high order solution for the added stability lobes in intermittent machining', in *Proceedings of the Symposium on Machining Processes*, Orlando, FL, (MED-11), 2000, pp. 871–878.

17. Zao, M. X. and Balachandran, B., 'Dynamics and stability of milling process', *International Journal of Solids and Structures* **38**, 2001, 2233–2248.
18. Bayly, P. V., Mann, B. P., Schmitz, T. L., Peters, D. A., Stépán, G., and Insperger, T., 'Effects of radial immersion and cutting direction on chatter instability in end-milling', in *Proceedings of ASME Engineering Congress and Exposition,* New Orleans, LA, 2002.
19. Mann, B. P., Insperger, T., Bayly, P. V., and Stépán, G., 'Stability of up-milling and down-milling, Part 2: Experimental verification', *International Journal of Machine Tools and Manufacture* **43**, 2003, 35–40.
20. Insperger, T., Mann, B. P., Stépán, G., and Bayly, P. V., 'Stability of up-milling and down-milling, Part 1: Alternative analytical methods', *International Journal of Machine Tools and Manufacture* **43**, 2003, 25–34.
21. Insperger, T., Stépán, G., Bayly, P. V. , and Mann, B. P., 'Multiple chatter frequencies in milling processes', *Journal of Sound and Vibration* **262**, 2003, 333–345.
22. Balachandran, B., 'Non-linear dynamics of milling process', *Philosophical Transactions of the Royal Society of London A* **359**, 2001, 793–819.
23. Bayly, P. V., Halley, J. E., Davies, M. A., and Pratt, J. R., 'Stability analysis of interrupted cutting with finite time in the cut', in *Proceedings of ASME Design Engineering Technical Conference, Manufacturing in Engineering Division*, Orlando, FL, 2001.
24. Bayly, P., Halley, J., Mann, B., and Davies, M., 'Stability of interrupted cutting by temporal finite element analysis', *Journal of Manufacturing Science and Engineering* **125**, 2003, 220–225.
25. Stépán G., 'Modelling nonlinear regenerative effects in metal cutting', *Philosophical Transactions of the Royal Society of London A* **359**, 2001, 739–757.
26. Davies M. and Burns, T., 'Thermomechanical oscillations in material flow during high-speed machining', *Philosophical Transactions of the Royal Society of London A* **359**, 2001, 821–846.
27. Grabec, I., 'Chaotic dynamics of the cutting process', *International Journal of Machine Tools and Manufacture* **28**, 1988, 19–32.
28. Altintas, Y. and Budak, E., 'Analytical prediction of stability lobes in milling', *CIRP Annals* **44**(1), 1995, 357–362.
29. Hanna, N. H. and Tobias, S. A., 'A theory of nonlinear regenerative chatter', *Journal of Engineering for Industry* **96**, 1974, 247–255.
30. Nayfeh, A. H., Chin, C. M., and Pratt, J., '*Applications of Perturbation Methods to Tool Chatter Dynamics*', in *Dynamics and Chaos in Manufacturing Processes*, Wiley, New York, 1997.
31. Stephenson, D. A. and Agapio, J. S., *Metal Cutting Theory and Practice*, 1st edn., Marcel Dekker, New York, 1997,
32. Jaluria, Y., *Computational Heat Transfer*, 1st edn., Hemisphere Publishing Corporation, Washington, 1986.
33. Peters, D. A. and Idzapanah, A. P., 'HP-version finite elements for the space-time domain', *Computational Mechanics* **3**, 1988, 73–78.
34. Virgin, L. N., *Introduction to Experimental Nonlinear Dynamics*, Cambridge University Press, Cambridge, UK, 2000.
35. Yamamoto, T. and Ishidam, Y., *Linear and Nonlinear Rotordynamics*, Wiley Series in Nonlinear Science, Wiley, New York, 2001.
36. Xie, A. and Dai, H., 'On the sensitivity of multiple eigenvalues of nonsymmetric matrix pencils', *Linear Algebra and Its Applications* **374**, 2003, 143–158.